Vibrational Spectroscopy of a Keggin Polyoxometalate on Metal Electrode Surfaces

Craig M. Teague, Xiao Li, Mary Ellen Biggin, Lien Lee, Jongwon Kim, and Andrew A. Gewirth*

Department of Chemistry and Fredrick Seitz Materials Research Laboratory, 600 S. Mathews Avenue, Urbana, Illinois 61801

Received: August 25, 2003; In Final Form: November 30, 2003

Polarization modulation infrared reflection−absorption spectroscopy and surface-enhanced Raman spectroscopy are used to interrogate the behavior of the Keggin-type polyoxometalate α-$[SiW_{12}O_{40}]^{4-}$ on Ag and Au electrode surfaces. Assignment of specific vibrational modes and their behavior as a function of potential show that α-$[SiW_{12}O_{40}]^{4-}$ adsorbs strongly on Ag but not on Au. On Ag, analysis of the potential-dependent spectroscopy provides insight into the behavior of this species on the electrode surface, especially at cathodic potentials. In particular, the spectroscopy shows that the molecule reorients on the Ag electrode surface at the potential where a voltammetric wave is found in the solution-based voltammetry. This reorientation inhibits the oxidation of the Ag surface-confined species.

1. Introduction

Polyoxometalates are discrete metal-oxide cluster compounds that exhibit interesting properties.[1−4] For example, these compounds can accept a number of electrons without major structural changes,[1,5,6] be highly charged in solution,[1,5] be easily functionalized with respect to redox properties and appending groups,[1,5,7,8] and be used as multidentate ligands.[1,8] This unique combination of desirable properties has led to polyoxometalates being used as homogeneous and heterogeneous catalysts,[5,9−11] superacids, corrosion protectors, and models for bulk metal oxides among many other potential applications.[12] Recent examples of the use of polyoxometalates in catalysis include the oxidation of lignin with O_2 in water[13] and the selective, efficient epoxidation of olefins with H_2O_2.[14]

Another attractive feature of polyoxometalates is their many possible structures.[1] One class of polyoxometalates is the heteropolyanions, where an atom of one type is encapsulated in a metal oxide framework of a different metal. Many different atoms can serve as the heteroatom, while the metal oxide framework most commonly contains predominantly Mo or W. Perhaps the best characterized heteropolyanions are the α-Keggin ions, which take the form α-$[XM_{12}O_{40}]^{n-}$ where X = a heteroatom with tetrahedral coordination to four O atoms, M = Mo or W in the +6 oxidation state, where each M atom is in a distorted octahedral coordination of O atoms with neighboring octahedra sharing edges or corners, and *n* is determined by the identity and oxidation state of the heteroatom.[1,15] Of the α-Keggin ions, the species studied most often have X = P or Si, and one of these, α-$[SiW_{12}O_{40}]^{4-}$, is used in this work as the acid form. This species is fully deprotonated and stable in acidic solution,[1] and the structure of this anion showing the four types of O atoms is shown in Figure 1.

The catalytic utility of polyoxometalates has motivated several groups to examine the association of these molecules with surfaces.[5,16] These studies have included electrodeposition;[17,18] studies on C,[19−24] Au,[20,25] and Hg[26] surfaces; well-characterized monolayer self-assembly;[27−30] and multilayer electrostatic assemblies utilizing surfaces derivitized by multicationic species.[31−35] In previous studies, we showed that a monolayer of α-$[SiW_{12}O_{40}]^{4-}$ self-assembles on Ag[27−30] and Au[29] surfaces with structures that could be explained using simple coordination ideas. In addition, we showed that α-$[SiW_{12}O_{40}]^{4-}$ exhibits a remarkably strong interaction with Ag surfaces in particular, as demonstrated by scanning tunneling microscopy (STM),[27−30] X-ray scattering,[30] and electrochemical[36] measurements. We also examined derivatives of α-$[SiW_{12}O_{40}]^{4-}$ including the lacunary species[37] α-$[SiW_{11}O_{39}]^{8-}$ and the substituted species[38,39] α-$[PVW_{11}O_{40}]^{4-/5-}$, where different oxidation states on V were utilized. In the latter case, it was shown that the reduced species α-$[PVW_{11}O_{40}]^{5-}$ was present on Ag surfaces regardless of the oxidation state of the species in solution; i.e., when either α-$[PVW_{11}O_{40}]^{4-}$ or α-$[PVW_{11}O_{40}]^{5-}$ was present in solution, only the reduced species is adsorbed on the surface.[38,39]

The electrochemical behavior of α-$[SiW_{12}O_{40}]^{4-}$ confined to Ag surfaces is unique in many respects. For example, we found[36] that the first redox wave of α-$[SiW_{12}O_{40}]^{4-}$, expected at about −0.2 V vs Ag/AgCl, was absent on Ag surfaces. However, the second wave at about −0.44 V was observed on Ag as a surface-confined redox couple. To explain this behavior, we speculated that the α-$[SiW_{12}O_{40}]^{4-}$ was reduced to α-$[SiW_{12}O_{40}]^{5-}$ on the Ag surface. The behavior of α-$[SiW_{12}O_{40}]^{4-}$ on Au(111) was substantially different; on this surface, the first redox wave was present and shown to be consistent with the solution-based redox couple.

In this study, we seek to explore the strong interaction of α-$[SiW_{12}O_{40}]^{4-}$ with Ag surfaces in more detail by utilizing surface-enhanced Raman spectroscopy (SERS), a surface-sensitive vibrational spectroscopy.[40−42] We correlate the SERS with the voltammetry in order to understand the origin of the missing wave found with the Ag surface-confined species. On the basis of these results, a model for the behavior of the adsorbed polyoxometalate as a function of potential is proposed. Furthermore, we contrast the vibrational spectroscopy of α-$[SiW_{12}O_{40}]^{4-}$ on Ag with that from the Au surface, where

* To whom correspondence should be addressed. Email: agewirth@uiuc.edu. Tel: 217-333-8329. Fax: 217-333-2685.

10.1021/jp036533m CCC: $27.50
Published on Web 01/16/2004

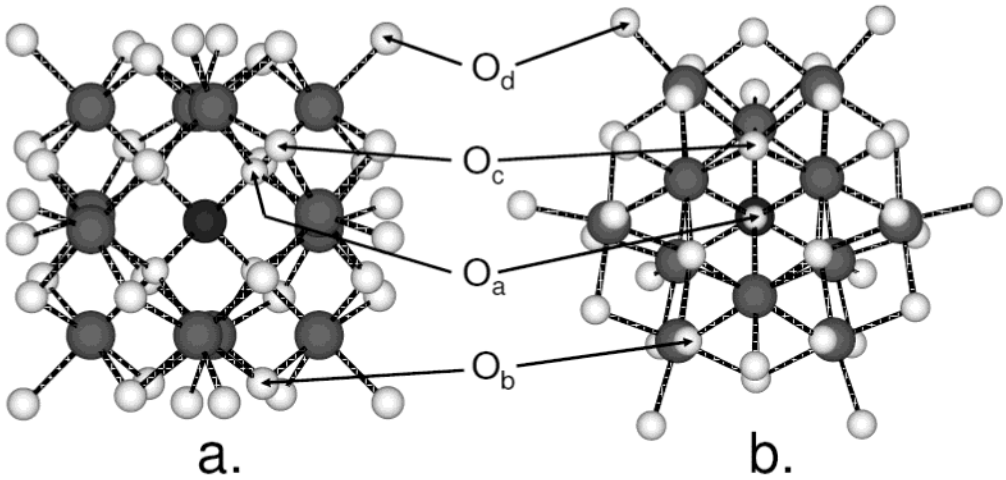

Figure 1. Two schematic views of α-$[SiW_{12}O_{40}]^{4-}$ where larger gray balls are W, small light gray balls are O, and black central ball is Si. (a) Viewed along an S_4 axis; (b) viewed along a C_3 axis. The four types of O atom are shown. O_a atoms are bonded to Si and weakly bonded to three W atoms which form a W_3O_{13} triad; a triad is best seen in part b as the three W atoms which are unobscured. O_b atoms are bonded to two W atoms from different triads; W−O_b−W forms an intertriad bridge. O_c atoms are bonded to two W atoms within the same triad; W−O_c−W forms an intratriad bridge. O_d atoms are bonded to one W atom as an oxo group W═O_d.

previous work has shown similar surface structures[29] but weaker interactions[29,36] occur.

2. Experimental Section

The α-$H_4SiW_{12}O_{40}$·nH_2O was synthesized using an established procedure.[7] Chemicals used in the synthesis were Na_2SiO_3·$5H_2O$ (Alfa Aesar, technical grade), Na_2WO_4·$2H_2O$ (Alfa Aesar, 99.0−101.1%, ACS), and concentrated HCl (Fisher Certified ACS Plus). After recrystallization from water, the product identity and purity were confirmed by infrared and Raman spectroscopies, cyclic voltammetry (CV), and elemental analysis.[7,15]

All solutions were prepared with Milli-Q water (Millipore, Inc., Milli-Q UV Plus, 18.2 MΩ cm). The supporting electrolyte was made using $HClO_4$ (J. T. Baker ULTREX II). Crystals (Monocrystals Co., 99.999+%, 1-cm diameter) of the desired metal were mechanically polished with α-Al_2O_3 of successively smaller grit sizes with sonication between grit sizes. For CV and polarization modulation infrared reflection−absorption spectroscopy (PM-IRRAS) experiments, Ag(111) single crystal surfaces were then chemically polished by using a literature procedure.[43] CV experiments utilized Ag(111) single crystals or Ag(111)/mica evaporated in a bell jar system and Au(111)/glass samples (Dirk Schröer, Inc.). The Au samples were flame annealed in a H_2 flame prior to use.[44]

Raman experiments, including SERS, were carried out in the Laser Laboratory of the Frederick Seitz Materials Laboratory at the University of Illinois as described previously.[45] SERS-active Ag surfaces were prepared as described by Weaver.[46,47] The excitation wavelength for Ag was 514.5 nm, provided from a I-90 Ar^+ laser (Coherent). SERS-active Au surfaces were prepared as reported previously.[45,48,49] For the Au surface, a CR-599 DCM dye laser (Coherent) pumped by the 514.5-nm line of a Series 2000 Ar^+ laser (Spectra Physics) provided the Raman excitation at 668.0 nm. Generally, the first spectrum was recorded at 0.0 V after the system had equilibrated for 2 min. The potential was then scanned negatively to −0.10 V, where the system was allowed to equilibrate for 2 min before another spectrum was taken. This continued until the desired cathodic limit was reached, whereupon the same procedure was used on the subsequent anodic scan. After the desired anodic limit was reached, the potential cycle was concluded by returning to 0.0 V using the same procedure. Spectra are presented here without background correction.

PM-IRRAS experiments were performed using a Magna-IR System 550 spectrometer (Nicolet) as described previously.[50,51] The solutions were purged with Ar prior to and during experiments. Spectra were collected at 4 cm^{-1} resolution. Twenty sets of 10 average scans and 50 difference scans each were taken, and the 20 sets were then averaged together.

CV experiments were carried out on an AFRDE5 (Pine Instruments) potentiostat by using a two-compartment glass cell with a Au wire as the counter electrode. The reference electrode, Ag/AgCl, was connected via a capillary salt bridge to minimize possible contamination. All solutions were purged with Ar for at least 20 min, and an Ar atmosphere was maintained in the cell during electrochemical experiments. All potentials are quoted vs Ag/AgCl in this work.

X-ray photoelectron spectroscopy (XPS) was performed on a PHI 5400 spectrometer (Physical Electronics) or an Axis Ultra spectrometer (Kratos) in the Center for Microanalysis of Materials of the Frederick Seitz Materials Research Laboratory at the University of Illinois.

The vibrational spectrum of the polyoxometalate was calculated using the IR/Raman spectrum calculation package within the MSI-Cerius^2 program suite.[52] Forces on the molecule are calculated by a quasiharmonic approximation, and the second-derivative matrix (Hessian) is used to calculate the vibrational modes.

3. Results

3.1. Cyclic Voltammetry. Figure 2 shows the voltammetry obtained from a solution containing 0.5 mM α-$[SiW_{12}O_{40}]^{4-}$ + 0.1 M $HClO_4$ on three different electrode surfaces. On highly oriented pyrolytic graphite (HOPG), three redox waves are observed; this voltammogram matches well with previously reported studies.[17,53−55] On Au(111), the first redox wave is in the expected location. The cathodic limit was −0.5 V due to H_2 evolution; the other waves due to α-$[SiW_{12}O_{40}]^{4-}$ were not observed since they occur near −0.5 V or at more negative potentials. On both HOPG and Au(111), the anodic and cathodic wave splitting and wave intensity as a function of scan rate behave in a manner consistent with solution redox processes.

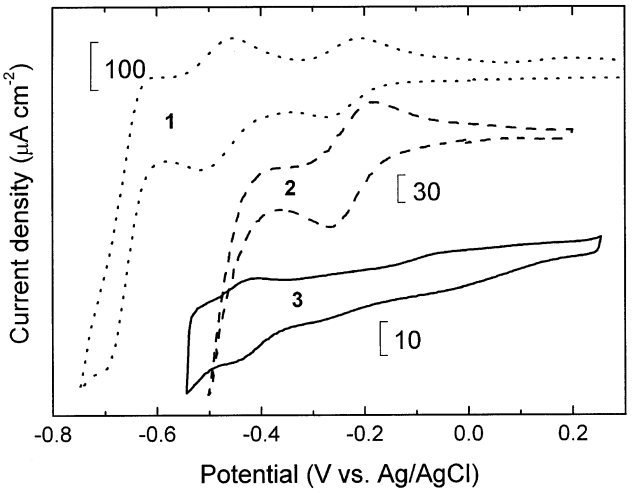

Figure 2. Cyclic voltammograms at 50 mV s^{-1} of 0.5 mM α-$[SiW_{12}O_{40}]^{4-}$ + 0.1 M $HClO_4$ at various electrodes. Curve 1 (dotted line), HOPG; curve 2 (dashed line), Au(111); curve 3 (solid line), Ag(111), fifth potential cycle. Curves have different current density scales and are offset from each other.

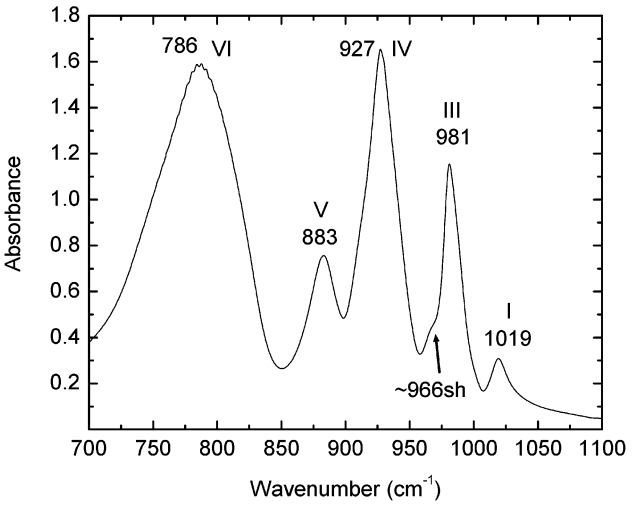

Figure 3. FTIR spectrum of α-$H_4SiW_{12}O_{40}$·nH_2O in a KBr pellet. Comparisons with literature data and assignments are given in Table 1.

On Ag(111), the response is quite different. As discussed previously, the first redox wave, expected at −0.2 V, is missing. However, the second wave at −0.44 V is present. Additionally, this wave is found to be associated with a surface-confined species.[36]

3.2. Infrared Spectroscopy. *3.2.1. Solid α-$H_4SiW_{12}O_{40}$·nH_2O.* Figure 3 shows the transmission IR spectrum for solid α-$H_4SiW_{12}O_{40}$·nH_2O in a KBr pellet. This spectrum matches well with literature observations,[15] as shown in Table 1.

3.2.2. PM-IRRAS of α-$[SiW_{12}O_{40}]^{4-}$ + $HClO_4$ on Ag(111). Figure 4 shows PM-IRRAS spectra for Ag(111) in 1 mM α-$[SiW_{12}O_{40}]^{4-}$ + 0.1 M $HClO_4$ as the potential was stepped from +0.20 to −0.60 V (Figure 4a) and from −0.60 to +0.20 V (Figure 4b). The potential was held constant while each set of spectra was collected. For clarity, the spectra have all been ratioed to the PM-IRRAS spectrum of Ag(111) in 0.1 M $HClO_4$ at open circuit. At +0.20 V, there are peaks at 1018, 982, 938, and 823 cm^{-1}, labeled I, III, IV, and VI, respectively. Upon stepping to negative potentials, peaks III and IV shift to lower energies and decrease in intensity. Interestingly, peaks I and VI broaden and disappear at negative potentials, although some residual intensity from peak VI can be seen at −0.6 V. Additionally, there is some intensity which could be due to band V at −0.6 V. Upon stepping back to positive potentials, peaks I and VI reappear. The relative intensity of peaks III and IV change so that while peak III is less intense than peak IV at +0.2 V, the opposite is the case at −0.6 V.

A plot of peak position vs potential for bands III and IV is shown in Figure 5. The two peaks exhibit different slopes between −0.20 V and −0.60 V. Peak III shows a Stark shift of 32.5 cm^{-1} V^{-1}, while peak IV shows a Stark shift of 52.5 cm^{-1} V^{-1}.

One of the most problematic features of in situ IRRAS spectroscopy is that the surface selection rule, which discriminates surface-associated molecules from those in solution, breaks down within about one-third to one-fourth of the wavelength of light used.[56] In the present case, this means that discrimination between molecules on the surface and those ca. 1 μm away from the surface is problematic. Nonetheless, the presence of a Stark shift and the absence of the band at 883 cm^{-1} (peak V) in the IRRAS suggest strongly that the majority of the information in the spectra shown in Figure 4 arise from surface-associated species.

3.3. Raman Spectroscopy. *3.3.1. Solid and Solution α-$[SiW_{12}O_{40}]^{4-}$ Raman Spectra.* Figure 6 shows normal Raman spectra obtained from solid α-$H_4SiW_{12}O_{40}$·nH_2O (Figure 6 bottom) and from a solution containing 0.1 M α-$[SiW_{12}O_{40}]^{4-}$ + 0.1 M $HClO_4$ (Figure 6 top). The solution spectrum was obtained in 0.1 M $HClO_4$ because α-$[SiW_{12}O_{40}]^{4-}$ remains intact at this pH.[1,7] By comparison with a spectrum obtained from a solution containing only 0.1 M $HClO_4$, the peak at 931 cm^{-1}, marked with an asterisk, is associated with perchlorate and is assigned to the Cl−O symmetric stretch.[57]

The spectrum of the solid material matches well with that previously reported,[15] as shown in Table 1. The solid spectrum shows a very intense peak, labeled II in Figure 6, with a shoulder I, although the precise location of this shoulder is difficult to determine. Peaks near IV and V constitute a broad feature and other bands may be present within this manifold. There is another broad feature, peak VII, which appears to contain at least two bands. Peaks VIII, IX, and X are very weak. Between 200 and 240 cm^{-1}, another group of peaks is present, with the most intense peak at 218 cm^{-1}. Below 200 cm^{-1}, there is a final group of peaks with the peak at 156 cm^{-1} most intense.

There is good general agreement between the solid and solution spectra indicating that α-$[SiW_{12}O_{40}]^{4-}$ is not decomposed in the solution used here, as expected.[1,7] Peaks from both spectra are tabulated in Table 1, which also gives literature values and assignments. As discussed in the literature,[58,59] there are some 44 Raman-allowed bands in α-$[SiW_{12}O_{40}]^{4-}$. Only a few of those modes are seen as discrete bands in the spectra reported here. There is considerable spectral congestion in the region between 900 and 1000 cm^{-1} and in bands at lower energies. Both IR studies[15] and calculations[59] indicate that there are Raman-allowed bands in the region between 600 and 850 cm^{-1}. However, neither the solid nor the solution Raman exhibits these bands, as reported previously.[15,58] The reasons for this behavior are unknown.

3.3.2. SERS. 3.3.2.1. α-$[SiW_{12}O_{40}]^{4-}$ + $HClO_4$ on Ag. Figure 7 shows potential-dependent SERS obtained from a Ag electrode immersed in a solution containing 0.5 mM α-$[SiW_{12}O_{40}]^{4-}$ + 0.1 M $HClO_4$. The cycle was begun at 0.0 V and continued by stepping cathodically to −0.7 V, then anodically to +0.3 V, and finally cathodically back to 0.0 V. The spectra exhibit nine distinct peaks, labeled II−X in the figure. Energies of these peaks are given in Table 1.

TABLE 1: Vibrational Bands and Assignments for α-$[SiW_{12}O_{40}]^{4-}$

label	literature[15] solid[a]	exp solid[b]	exp soln	Ag IRRAS at +0.2 V	Ag SERS at 0.0 V	Au SERS at 0.0 V	band assignments[e]
I	1016 w, 1020 w IR	1017 sh, 1019 IR	1015 sh	1018 IR			asymmetric coupling of $\nu_{as}(Si-O_a)$, $\nu_{as}(W=O_d)$
II	1000 vs	998	996		992	990	$\nu_s(W=O_d)$[15,65]
III	975 m, 981 s IR	973, 981 IR, 966sh IR	979	982 IR	965	957	$\nu_{as}(W=O_d)$[15,65]
IV	923 w, 928 vs IR	920, 927 IR	916	938 IR	940, 913[c]	906	$\nu_{as}(Si-O_a)$, $\nu(W-O_b-W)$[15,65]; symmetric coupling of $\nu_{as}(Si-O_a)$, $\nu_{as}(W=O_d)$
V	880 vw, 880 m IR	893, 883 IR	893		881[d]	892	$\nu_{as}(W-O_b-W)$ mixed[15,65]
Va						850	
VI	785 vs IR	786 IR, ~666	~670	823 IR	792		$\nu_{as}(W-O_c-W)$ mixed[15,65]
VII	551 w	553, 538	553, 528		516	514	$\nu_s(W-O_c-W)$ mixed[65]
	538 w						$\nu_s(W-O_c-W)$ mixed[65]
VIII	458 vw	453	456		456		$\delta(W-O-W)$, likely mixed
IX	398 vw	373	373		369	397	$\delta(O_c-W-O_d)$,[15] $\delta(W-O-W)$ mixed
X	328 vw	328			333		δ mixed
		285	287				$\delta(O_c-W-O_d)$ mixed
	237 m	238	240 sh				$\delta(O_c-W-O_d)$ mixed
	222 m	218	220				$\nu_s(W-O_a)$, mixed including $\nu(W-O-W)$[15,65]
	207 m	205	205 sh				$\delta(W-O-W)$, $\delta(O-W-O)$
	174.5 m	176					$\delta(W-O-W)$, $\delta(O-W-O)$
	154 s	156	158 sh				$\delta(W-O-W)$, $\delta(O-W-O)$
			151				
	103 s	104	104				$\delta(W-O-W)$, $\delta(O-W-O)$
	87 s	91	89				$\delta(W-O-W)$, $\delta(O-W-O)$

[a] Relative intensities are given by vs = very strong, s = strong, m = medium, w = weak, vw = very weak, and sh = shoulder. [b] All band positions are in cm^{-1} and refer to Raman bands unless designated as IR. [c] At +0.3 V. [d] At −0.4 V. [e] Assignments are given by ν_s = symmetric stretch, ν_{as} = asymmetric stretch, δ = bend. See Figure 1 for atom-labeling scheme.

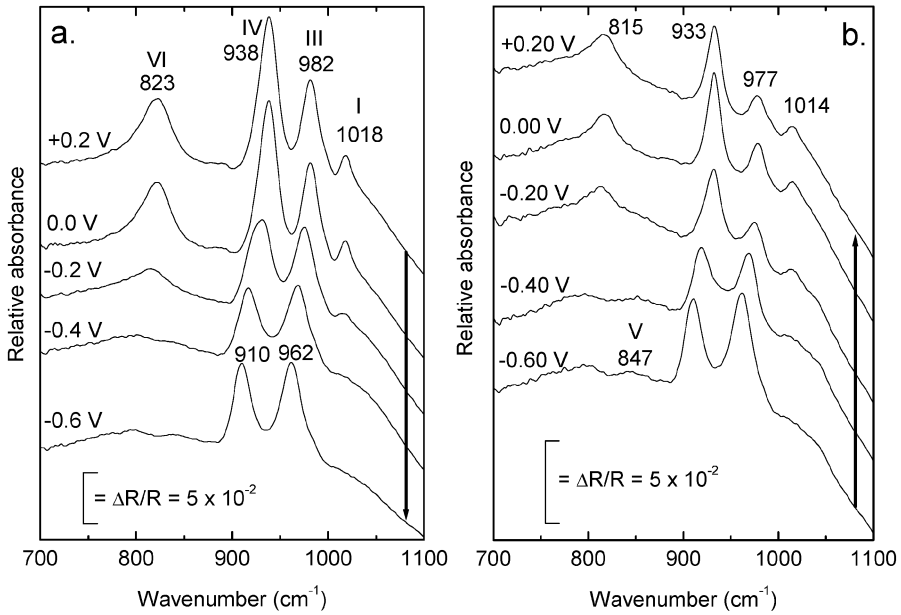

Figure 4. PM-IRRAS for Ag(111) in 1 mM α-$[SiW_{12}O_{40}]^{4-}$ + 0.1 M $HClO_4$ at various potentials, (a) negative-going steps, (b) positive-going steps. All spectra are ratioed to a spectrum of Ag(111) in 0.1 M $HClO_4$ at open circuit. Scale bars are shown in each panel.

The solid (Figure 6) and surface (Figure 7) spectra exhibit good overall correlation based on peak position, although the peak-intensity profiles sometimes differ between the solid and surface spectra. For example, peak II is found at 998 cm^{-1} in the solid spectrum and at 992 cm^{-1} at 0.0 V on the Ag surface. However, while peak II is more intense than peak III in the spectrum of the solid material, the opposite occurs on the Ag surface. Reversal of intensity for these two peaks has been noted previously for certain polyoxometalate species, including some α-Keggin species, in SERS studies of colloidal Ag particles aggregated with polyoxometalates.[60] Other peaks (III, IV, V) are redshifted on the surface by about 10 cm^{-1}, while peaks VIII, IX, and X are shifted little relative to the solid spectrum. On the other hand, peak VII is redshifted by roughly 30 cm^{-1} on the Ag surface relative to the solid spectrum. These correlations are summarized in Table 1.

There are two peaks, IV and VI, in Figure 7 that do not correlate well with the solid spectrum. Peak IV seems to contain at least two bands, one of which is present at 940 cm^{-1} at 0.0 V but decays quickly and disappears around −0.2 V. This peak is reacquired on the subsequent anodic sweep. The second component of this band appears around +0.1 V and becomes quite prominent, especially positive of +0.2 V where it appears at 913 cm^{-1}. On the other hand, peak VI grows in starting at −0.3 V and remains prominent at negative potentials. The origins of this band will be discussed below.

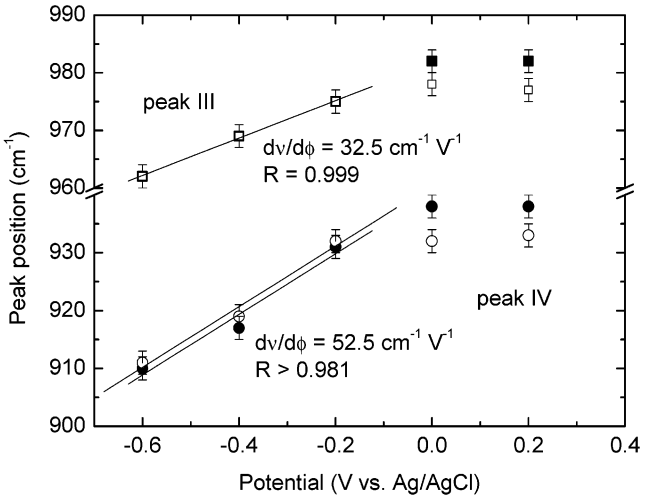

Figure 5. IRRAS peak positions for peaks III (squares) and IV (circles) as a function of potential for Ag(111) in 1 mM α-$[SiW_{12}O_{40}]^{4-}$ + 0.1 M $HClO_4$. Filled symbols are negative-going potential steps; open symbols are positive-going potential steps. Error bars represent instrumental uncertainty. The lines are linear fits to the data from −0.2 through −0.6 V; the slopes and correlation coefficients are given as well.

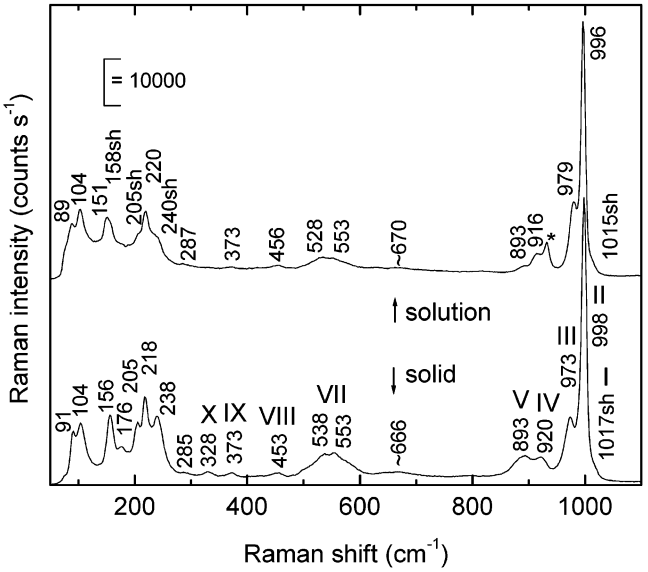

Figure 6. Raman spectra for solid α-$H_4SiW_{12}O_{40}$·nH_2O (bottom spectrum) and 0.1 M α-$[SiW_{12}O_{40}]^{4-}$ + 0.1 M $HClO_4$ (top spectrum). The peak marked with an asterisk, at 931 cm^{-1}, is due to ClO_4^-. Comparisons with literature data and assignments are given in Table 1.

SER spectra of 0.1 M $HClO_4$ on Ag absent α-$[SiW_{12}O_{40}]^{4-}$ exhibit a weak peak at 933 cm^{-1}, nearly the same location seen in the solution spectrum. This peak does not shift with potential, as reported previously,[61] and its intensity does not change appreciably relative to the background as the potential is varied. A second band of unknown origin grows in on the anodic sweep at 965 cm^{-1} and then disappears on the subsequent cathodic sweep without shifting position. The lack of shift with potential, present for both of these bands, usually indicates little or no direct interaction with the Ag surface.[61] The background intensity increased on the anodic sweep, especially past +0.2 V, and decayed slowly upon reversal of the potential cycle.

Figure 7 shows that the bands associated with α-$[SiW_{12}O_{40}]^{4-}$ on the Ag surface exhibit considerable potential dependence. In particular, peaks II, III, IV, and VII are more prominent at positive potentials while the very broad feature between 700 and 900 cm^{-1}, including peaks V and VI, is more prominent negative of −0.3 V. Furthermore, most peaks shift to lower energy during the cathodic sweep. These trends are generally reversible with potential and upon further potential cycling.

Since electrochemical,[36] STM,[27-30] and X-ray scattering[30] measurements have all suggested that α-$[SiW_{12}O_{40}]^{4-}$ forms a strong interaction with the Ag surface, it is reasonable to expect bands in the SER spectra to arise as a consequence of this interaction. Vibrations for Ag−O are typically found[62,63] in the region between 240 and 280 cm^{-1}, and SER spectra often showed a band in this region (not shown). However, there are bands due to α-$[SiW_{12}O_{40}]^{4-}$ present in this region, as seen in Table 1. Because of this spectral congestion, it is difficult to make any meaningful statement as to whether Ag−O vibrations are observed.

Figure 8 shows the potential dependence of peak position for peaks III and VI. For peak III, there are three distinct regions in the plot with the middle region between 0.0 V and −0.4 V exhibiting a linear Stark shift of 43 cm^{-1} V^{-1}. The high and low potential regions exhibit negligible shift with potential. This behavior is found for several other peaks including II, VII, and VIII, all of which show similar Stark shifts in the middle potential region.

Figure 8 shows that peak VI exhibits a somewhat different behavior. While there is more uncertainty in peak position due to the width of peak VI, Figure 8 shows that this peak also exhibits three distinct regions, where the middle region shows a roughly linear shift between 90 cm^{-1} V^{-1} (cathodic) and 150 cm^{-1} V^{-1} (anodic).

Other peaks show essentially no Stark shift (peak IX) or have at least two components that behave differently (peak IV), which precludes establishment of definitive peak shifts as a function of potential. Peak V shows little shift over the potential range where it is reasonably well resolved (−0.4 through −0.7 V). This peak may be present as a shoulder at more positive potentials, and if this behavior is included, this peak behaves roughly like peak III. Finally, peak X shows more scatter in the peak position as a function of potential. This peak may actually split at more cathodic potentials, but it is difficult to make definitive conclusions about this peak due to its very weak intensity.

Figure 9 shows the relative change in peak intensity for peaks III and VI as a function of potential. As seen qualitatively in Figure 7, peak VI exhibits a substantial increase in intensity at negative potential values. Upon cycling back to +0.2 V, this intensity decreases and then rises past +0.2 V. Peak III also exhibits an intensity decrease upon the anodic scan, but it also loses intensity on the cathodic scan as well. The intensities of both peaks III and VI are reversible between −0.4 and −0.7 V, but this is not so at more positive potentials, where there is considerable hysteresis in the relative peak intensity, with the anodic scan always being less intense than the cathodic scan. Both peaks exhibit relative intensity minima at −0.3 V on the cathodic scan but at +0.2 V on the anodic scan. Peaks II and VII behave in a manner similar to peak III, with an intensity maximum around 0 V on the cathodic scan. Peaks VIII, IX, and X show intensity maxima at more negative potentials, analogous to peak VI, although other comparisons involving these three peaks are difficult due to their being very weak or absent at more positive potentials. Interestingly, most peaks return to nearly the same relative intensity after the completion of one full potential cycle.

Peak IV appears somewhat anomalous relative to the peaks described above. It disappears quickly on the cathodic sweep but reappears on the anodic sweep and is very prominent at

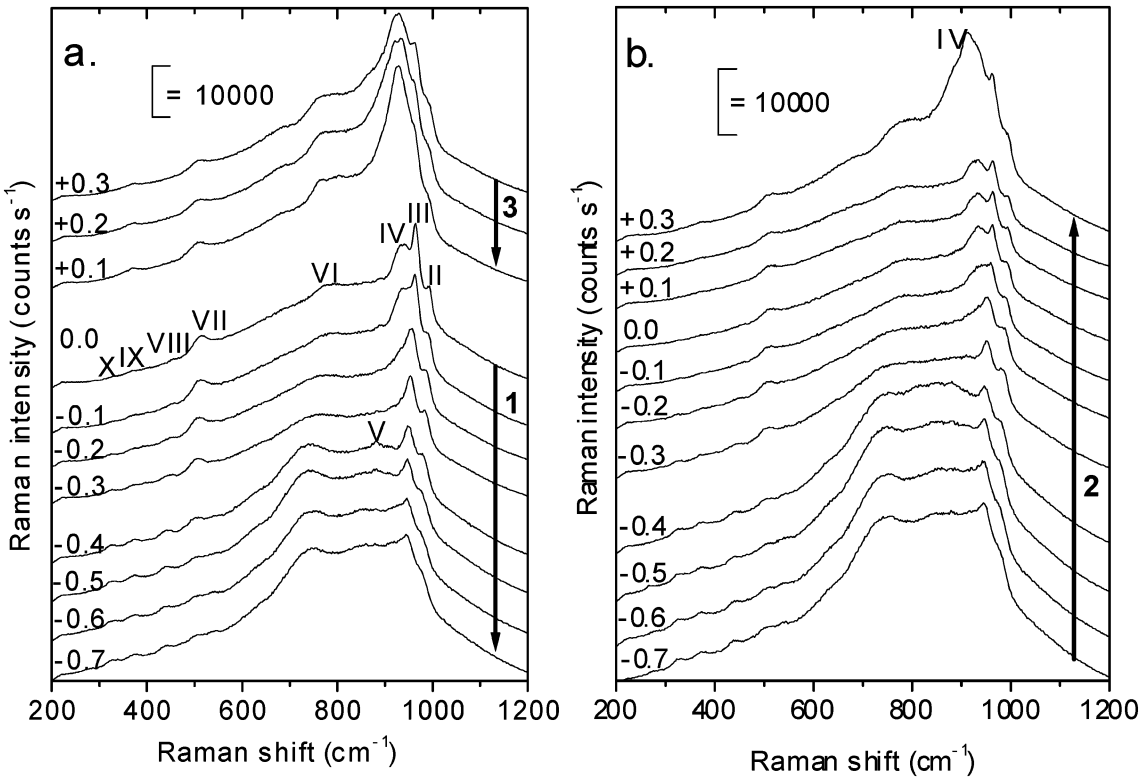

Figure 7. SER spectra for 0.5 mM α-$[SiW_{12}O_{40}]^{4-}$ + 0.1 M $HClO_4$ on Ag. The first complete potential cycle is shown, beginning and ending at 0.0 V. (a) Negative-going potential steps; (b) positive-going potential steps. Peak positions are given in Table 1.

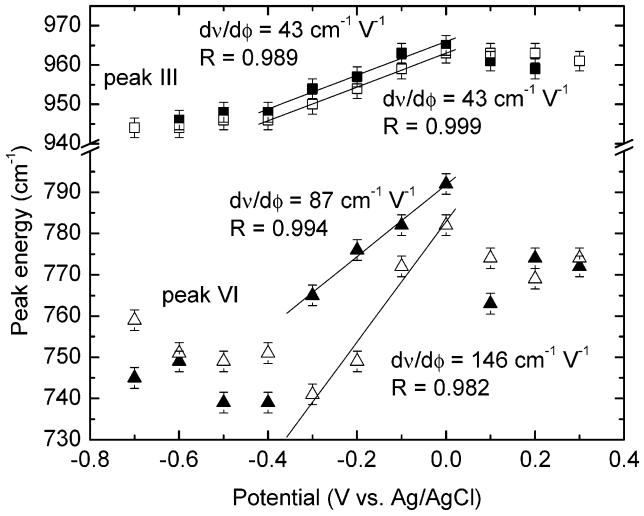

Figure 8. SERS peak positions for peaks III (squares) and VI (triangles) as a function of potential for Ag in 0.5 mM α-$[SiW_{12}O_{40}]^{4-}$ + 0.1 M $HClO_4$. Filled symbols are negative-going potential steps; open symbols are positive-going potential steps. One complete potential cycle is shown, as in Figure 7. Error bars represent instrumental uncertainty. Slopes and correlation coefficients are given for the linear regions of the plots.

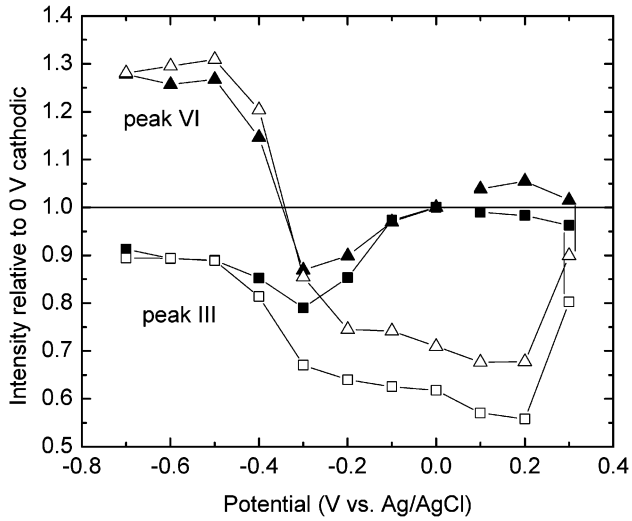

Figure 9. SERS relative intensities for peaks III (squares) and VI (triangles) as a function of potential for Ag in 0.5 mM α-$[SiW_{12}O_{40}]^{4-}$ + 0.1 M $HClO_4$. Filled symbols are negative-going potential steps; open symbols are positive-going potential steps. One complete potential cycle is shown, as in Figures 7 and 8. Each peak was referenced to its intensity at the beginning of the experiment (0.0 V cathodic).

+0.3 V on the anodic sweep in the first potential cycle. This peak loses intensity on the subsequent cathodic sweep, becoming a shoulder and then disappearing on the cathodic sweep of the second potential cycle. This peak reappears on the anodic sweep of the second potential cycle.

3.3.2.2. α-$[SiW_{12}O_{40}]^{4-}$ + $HClO_4$ on Au. To compare the interaction of α-$[SiW_{12}O_{40}]^{4-}$ between Ag and Au electrode surfaces, we obtained potential-dependent SERS from a Au surface in a solution containing 0.5 mM α-$[SiW_{12}O_{40}]^{4-}$ + 0.1 M HClO4, as shown in Figure 10. Spectra were recorded to a cathodic limit of −0.5 V only due to the onset of H_2 evolution. SER spectra on Au show generally less intense peaks relative to on Ag.

The spectra shown in Figure 10 exhibit seven distinct bands at 990 (peak II), 957 (peak III), 906 (peak IV), 892 (peak V), 850 (peak Va), 514 (peak VII), and 397 cm^{-1} (peak IX). Interestingly, the bands exhibit no potential dependence with regard to position and little difference (ca. 20%) with regard to relative intensity as a function of potential. This behavior stands in contrast to that found for Ag where potential-dependent relative intensity changes of about a factor of 2 are observed for peak VI.

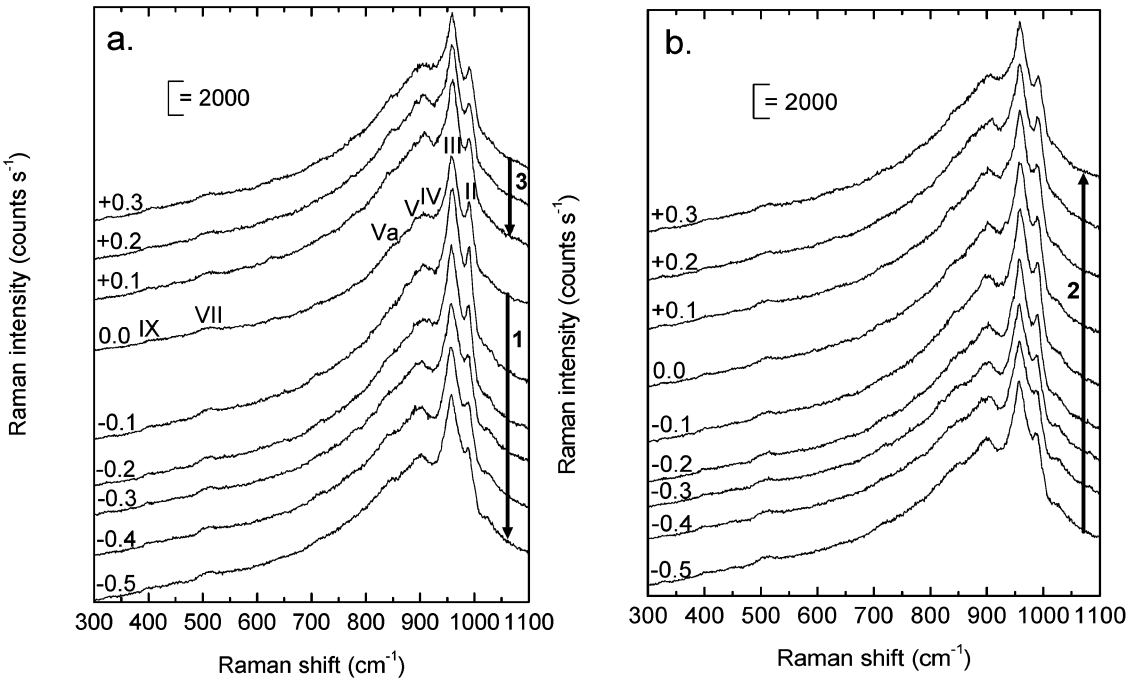

Figure 10. SER spectra for 0.5 mM α-$[SiW_{12}O_{40}]^{4-}$ + 0.1 M $HClO_4$ on Au. The first complete potential cycle is shown, beginning and ending at 0.0 V. (a) Negative-going potential steps; (b) positive-going potential steps. Peak positions are given in Table 1.

Comparison of peak positions for α-$[SiW_{12}O_{40}]^{4-}$ adsorbed on the Au and Ag surfaces at 0 V reveals a number of similarities. Both systems exhibit a high energy peak at ca. 990 cm^{-1} followed by an intense peak at ca. 960 cm^{-1} as well as a weaker, broad feature at ca. 515 cm^{-1}. The spectral structure at intermediate energies appears more complex on Ag relative to Au with a broad envelope of intensity between 700 and 900 cm^{-1}. However, where direct comparison is available, both systems have bands in the same region, as seen in Table 1.

4. Discussion

The data presented above provide considerable insight into the manner in which α-$[SiW_{12}O_{40}]^{4-}$ associates with the Ag electrode surface and the potential-dependent behavior of this molecule. In what follows, we address the correlation between the surface and solid spectra, the potential-dependent behavior of the molecule, and the differences in behavior between α-$[SiW_{12}O_{40}]^{4-}$ adsorbed on Au relative to Ag.

There are several major differences in the spectra of the α-$[SiW_{12}O_{40}]^{4-}$ molecule on the Ag surface relative to solid and solution spectra. First, it appears that the relative intensity of the symmetric and asymmetric W═O_d stretches (peaks II and III) are inverted in the SERS when compared with the solid. Second, the 883-cm^{-1} band (peak V) seen in the IR spectrum of the solid is missing in the PM-IRRAS. Third, the low-energy modes seen in the SERS around 516 cm^{-1} (peak VII) are redshifted by ca. 30 cm^{-1} relative to the solid. Fourth, the band around 820 cm^{-1} (peak VI) in the PM-IRRAS disappears as the potential is moved cathodically past −0.3 V while bands in the 700−900 cm^{-1} region, including peak VI, increase in intensity at the corresponding potentials in the SERS. Fifth, some, but not all, of the bands exhibit a large Stark detuning effect on Ag, but only over a specific potential range. Finally, α-$[SiW_{12}O_{40}]^{4-}$ adsorbed on the Ag surface exhibits considerably more potential dependent activity than is found with the same molecule adsorbed on Au.

4.1. Peak Assignments. We first address the present understanding of the vibrational spectroscopy of α-Keggin ions. The α-$[SiW_{12}O_{40}]^{4-}$ anion, which has T_d point group symmetry with all W atoms equivalent, has 153 normal modes which span $\Gamma_{vib} = 9a_1 + 4a_2 + 13e + 16t_1 + 22t_2$. Of these, 44 ($a_1 + e + t_2$) are Raman active and 22 (t_2) are infrared active, with the infrared active bands being coincident with Raman active bands. Several studies before 1985 used two distinct methods to assign the vibrations in α-Keggin species; a complete discussion and symmetry analysis of these two methods has been reviewed by Buckley and Clark.[58] Although the early studies did not always provide consistent assignments due to the size and complexity of the molecular species, a general consensus has emerged since about 1985.[58,59,64] This general consensus essentially agrees with the work of Rocchiccioli-Deltcheff and co-workers.[15,65] Recently, a nonempirical computational study based on density functional methods[59] has given calculated band positions, infrared intensities, and very detailed assignments for a number of α-Keggin polyoxometalates. This study confirmed the earlier assignments[15,58,65] for most bands, although in a few cases the existence of coupled vibrations between ν_{as}(Si—O_a) and ν_{as}(W═O_d) was suggested, where W═O_d corresponds to a terminal oxo group bound to one W atom only (see Figure 1). Coupled vibrations had not been discussed by previous workers. The computational study also noted, in agreement with earlier work,[15,58,64,65] that only some of the ν(W═O_d) bands can be considered pure stretches. Because of the complexity of the structure, nearly all other modes have mixed character. In addition, the specific assignments for the higher-energy modes are more certain than are the assignments for the lower energy modes, especially for the exact motions involved in the bending modes below about 200 cm^{-1}.

In the present study, there is good agreement with the literature values for peak positions and intensities for solid α-$H_4SiW_{12}O_{40}$ as noted in Table 1. Most peaks that do not match literature values exactly are weak or occur as shoulders. The assignments given in Table 1 are based on literature assignments where noted in the table. Where no reference is given in the table, these are proposed assignments. These assignments draw on the work by Bridgeman,[59] who proposed assignments for

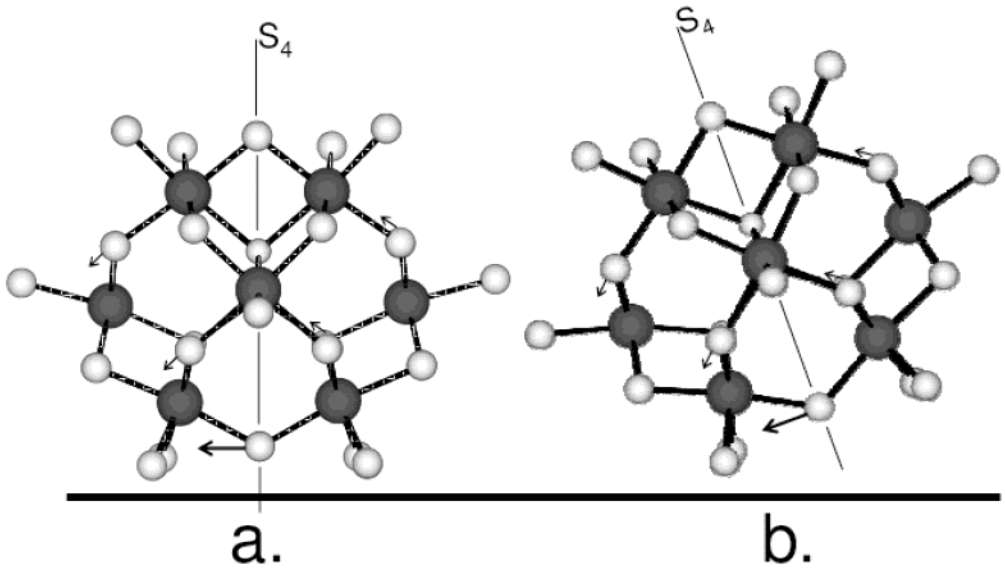

Figure 11. Schematic side views of α-$[SiW_{12}O_{40}]^{4-}$ on a Ag surface showing a t_2 vibrational mode likely responsible for peak V. Arrows show relative displacements of atoms. The major displacement for this mode is shown by the large arrows on O_b atoms near the bottom of the molecule. A second major arrow, on a separate O_b atom, is obscured from view immediately behind the first major arrow.

α-$[PW_{12}O_{40}]^{3-}$. Although the present work deals with α-$[SiW_{12}O_{40}]^{4-}$, most assignments for W−O modes are likely quite similar, as shown in previous spectroscopic studies,[15,58,65] especially if the Keggin anion is viewed as a clathrate of an anion inside a neutral cage $[XO_4]^{n-}$@$W_{12}O_{36}$ (X = Si, P) with relatively little covalency between the two fragments.[66]

4.2. Comparison of Solid and Surface-Confined α-$[SiW_{12}O_{40}]^{4-}$. Comparison of the Raman spectra in Figures 6 and 7 suggests strongly that α-$[SiW_{12}O_{40}]^{4-}$ is intact on the Ag surface. That both the symmetric and asymmetric W═O_d stretches are present and within ca. 10 cm^{-1} of their positions in the solid material suggests strongly that the surface-associated species is not degraded. Additionally, the high-energy modes seen in the PM-IRRAS are also close to their solid-state values. This inference is consistent with our understanding as developed using STM[27−30] and X-ray scattering[30] techniques. Raman spectra obtained from solid α-$Ag_4SiW_{12}O_{40}$·nH_2O also exhibit ca. 10 cm^{-1} redshifts in the W═O_d modes of the α-$[SiW_{12}O_{40}]^{4-}$ moiety.[67]

However, we note that the relative intensities of the symmetric and asymmetric W═O_d stretches on the Ag surface are inverted compared with the Raman spectrum of the solid material. This change in relative intensity, noted before in SERS of polyoxometalates on colloidal Ag particles,[60] likely reflects the different polarizability of these modes when the molecule is associated with the surface. In particular, the symmetric stretch will be inhibited through the agency of surface association.

Both the PM-IRRAS and the SERS provide information about the way in which the α-$[SiW_{12}O_{40}]^{4-}$ molecule is associated with the Ag surface. Interestingly, the 883 cm^{-1} band (peak V) seen in the solid-state IR spectrum shown in Figure 3 is absent in the IRRAS spectrum shown in Figure 4. The broad band, which maximizes at 786 cm^{-1} (peak VI), is also either absent or shifted to a narrower band which peaks at ca. 820 cm^{-1} on the surface. In the SER spectra, there is a dramatic increase in intensity in modes centered at 792 cm^{-1} (peak VI) relative to the corresponding spectrum of the solid material. Additionally, bands around 540−550 cm^{-1} (peak VII) in the solid material are redshifted nearly 30 cm^{-1} on the Ag surface.

We next examine the spectral origin of these bands. By reference to Table 1, all of these bands are in an energy region associated with stretches for either W−O_c−W or W−O_b−W bridging modes, where W−O_c−W corresponds to a bridging O group between two W atoms in the same triad and W−O_b−W corresponds to a bridging O group between two W atoms in different triads (see Figure 1). The fact that these modes are altered both in energy and intensity while the energies of modes corresponding to the W═O_d stretches are not strongly affected suggests that the molecule interacts with the surface by association through W−O_c−W and W−O_b−W bridging modes.

The disappearance of the peak V in the IR spectrum upon surface association suggests that this mode no longer has a component normal to the surface. We note that the peak V is still present in some of the SER spectra, so it is not likely that this band has simply moved to a different energy.

We performed calculations to find the vibrational modes of the polyoxometalate, the results of which indicated that there were a number of t_2 symmetry modes in the region between 1000 and 750 cm^{-1}. By reference to the much more complete DFT calculation[59] as well as previous spectroscopic studies,[15,58,65] we assign the 883 cm^{-1} band, peak V, to predominately W−O_b−W asymmetric stretch modes that exhibit considerable displacement normal to an S_4 axis of the α-$[SiW_{12}O_{40}]^{4-}$ molecule. Figure 11 shows a likely candidate for the mode largely responsible for this band. The figure shows that the major displacements associated with the vibration for one of the components of this t_2 mode are along the arrows indicated. When the α-$[SiW_{12}O_{40}]^{4-}$ molecule associates with the Ag surface with an S_4 axis perpendicular to the surface, as suggested from analysis of both STM[27−30] and X-ray-reflectivity[30] measurements, this mode is predominately parallel to the surface, as shown in Figure 11a. We thus anticipate little intensity in the infrared.

In the SERS, the bands in the region between 500 and 550 cm^{-1} (peak VII) are substantially redshifted compared with their solid-state counterparts. These peaks are associated predominantly with W−O_c−W symmetric stretch modes. This red shift may be reflective of loss of electron density in the W−O_c−W bond upon surface coordination.

4.3. Potential-Dependent Behavior. One of the most interesting features regarding α-$[SiW_{12}O_{40}]^{4-}$ confined to Ag

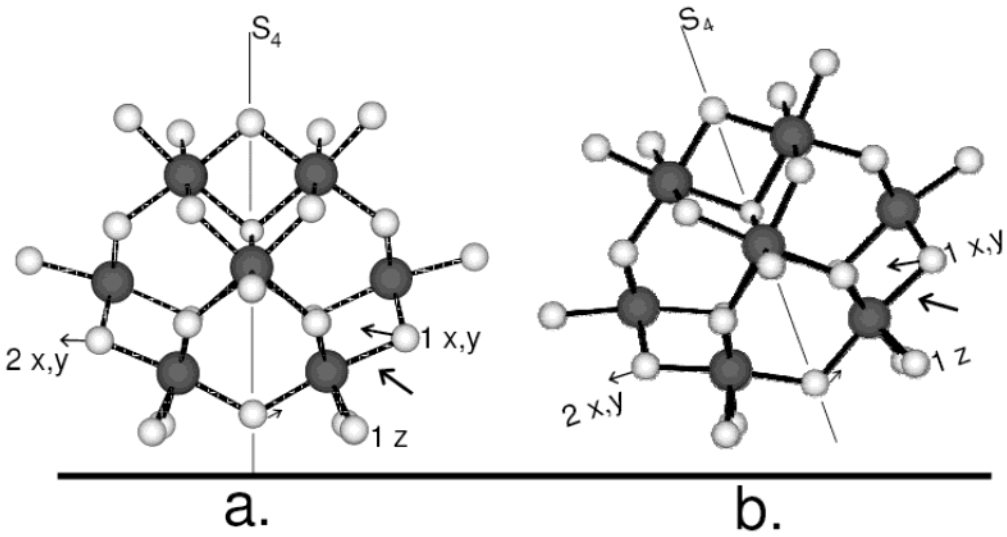

Figure 12. Schematic side views of α-$[SiW_{12}O_{40}]^{4-}$ on a Ag surface showing a t_2 vibrational mode likely responsible for peak VI. Arrows show relative displacements of atoms. The major displacement for this mode is controlled by O_c atoms labeled 1, where one of these (1*y*) is obscured by 1*x* and one (1*z*) is partially obscured by an O_d atom. There is also some contribution from O_c atoms labeled 2, one of which (2*y*) is obscured by 2*x*. The large arrow outside the molecule shows the overall displacement obtained from combining vectors 1*x*, 1*y*, and 1*z*, where the vector for 1*y* is obscured by the vector for 1*x* and the vector for 1*z* is obscured by W−O bonds.

surfaces is the absence of the voltammetric wave seen in solution at −0.2 V vs Ag/AgCl. In a previous paper, we speculated that this wave was shifted anodically to beyond the potential of Ag dissolution.[36] There is precedent in the literature for redox waves of adsorbed species being shifted positive relative to their solution waves.[68]

Stated another way, we suggested that the α-$[SiW_{12}O_{40}]^{4-}$ molecule was reduced on the Ag surface. We showed that a α-$[SiW_{12}O_{40}]^{4-}$ derivative α-$[PVW_{11}O_{40}]^{n-}$ was in fact reduced upon its association with an Ag surface.[38,39] In their work with Ag colloids, Siiman and Feilchenfeld noted distinct changes when α-$[SiW_{12}O_{40}]^{4-}$ was added to the Ag sol.[60] The authors attributed these changes to a chemical redox reaction between α-$[SiW_{12}O_{40}]^{4-}$ and elemental Ag to yield a Ag(I) species.

To check whether the α-$[SiW_{12}O_{40}]^{4-}$ molecule is reduced, we performed two additional measurements. First, we examined the XPS of α-$[SiW_{12}O_{40}]^{4-}$ on Ag. On the Ag surface, α-$[SiW_{12}O_{40}]^{4-}$ exhibits peaks associated with the W $4f_{5/2}$ and $4f_{7/2}$ levels. The position of the characteristic $4f_{7/2}$ line was 36.4 eV, which is consistent with W in the +6 oxidation state. If one of the W atoms was reduced to the +5 level, a shift to a value of ca. 35.7 eV is expected.[69] Unfortunately, the line width (full width at half maximum) of the $4f_{7/2}$ transition was 1.1 eV, which makes this shift unobservable.

Second, we obtained normal Raman spectra of the one-electron-reduced α-$[SiW_{12}O_{40}]^{5-}$ molecule. The α-$[SiW_{12}O_{40}]^{4-}$ molecule was reduced electrochemically by poising the potential of a Au electrode to −0.35 V. After ca. 2 h, the solution exhibited the characteristic deep-blue color of the reduced species.[1] This color persisted for at least 0.5 h following the removal of potential control, transfer of solution to the Raman cuvette, and acquisition of spectra. However, spectra of the reduced species were nearly identical with those obtained from the oxidized form, especially in the well-resolved W═O_d region. This result is in accord with previous IR studies[70,71] of the one-electron-reduced α-Keggin species α-$PMo_{12}O_{40}^{4-}$, although one of these studies showed dramatic changes in the IR spectrum of the two-electron-reduced molybdate species. This observation unfortunately does not allow us to assign an oxidation state (either fully oxidized or one-electron reduced) to the molecule on the surface.

However, we note that Figure 2 shows that the voltammetric wave for subsequent reduction of the surface-confined α-$[SiW_{12}O_{40}]^{4-}$ molecule is within 20 mV of its solution value.[36] We would expect that if the molecule existed on the surface in oxidized form that this wave would be substantially shifted to more cathodic values. More reasonably, we expect that the molecule is reduced upon association with the Ag surface. The question then becomes why the −0.2 V wave is absent on the subsequent anodic scan. This question is addressed by the vibrational spectroscopic data, which show that the molecule undergoes substantial changes at this potential, as we discuss in the next section.

4.3.1.Changes in Peak Intensities. There are changes in both the SERS and the PM-IRRAS at −0.2 V that provide some insight into the origin of the disappearance of the corresponding voltammetric wave. First, the SERS shows that the modes associated with peak VI increase dramatically in intensity after a potential of −0.3 V is reached on the cathodic scan. Figure 9 shows that the relative intensity of these modes increases by about a factor of 2. However, this behavior is not found for all modes associated with α-$[SiW_{12}O_{40}]^{4-}$ on the Ag surface. By way of contrast, the modes associated with peak III and several other peaks are nearly constant in intensity in this potential region. Increase in SERS intensity can arise from many sources; however, a likely origin of this behavior is reorientation of the molecule such that the modes associated with peak VI are closer to the surface, where they are more easily enhanced through interaction with the surface plasmon.

The PM-IRRAS also exhibits potential-dependent behavior. Figure 4 shows that when the potential is moved to values negative of −0.3 V that peak VI loses considerable intensity. Since this band must be a vibration of t_2 symmetry, we again examine the calculation to ascertain what displacements are responsible for this mode. Figure 12 shows a likely candidate. This mode, predominantly due to W−O_c−W asymmetric stretching, has considerable displacement perpendicular to an S_4 axis, but it also has some displacement parallel to this axis. With an S_4 axis perpendicular to the surface, as shown in Figure 12a, this mode exhibits its predominant motion at about 40° relative to the surface. If the molecule were to rotate slightly to roughly the position shown in Figure 12b, this angle would

become much smaller, resulting in a loss of most of the component normal to the surface and attendant attenuation in the IRRAS intensity.

Upon rotation on the surface as shown in Figure 12b, the mode likely responsible for peak V (discussed above, shown unrotated in Figure 11a) will of course rotate as well. However, after rotation, the major displacement of this mode still forms a relatively small angle with the surface leading to minimal intensity in the IRRAS even after rotation. This mode is shown after rotation in Figure 11b. We note that the intensities of both of these bands are not strictly zero past −0.3 V as shown in Figure 4, but the rotation shown in Figures 11b and 12b could account for both the absence or near absence of peak V and the potential-dependent intensity changes in peak VI in the IRRAS.

The rotation shown in Figures 11b and 12b would also bring two $W-O_c-W$ moieties closer to the surface, labeled as 2 in Figure 12. This could account for the increase in SERS intensity for modes associated with asymmetric stretching of these bonds as discussed above.

4.3.2. Stark-Shift Behavior. As seen in Figure 5, different peaks exhibit different Stark shifts in the IRRAS over the range −0.2 through −0.6 V. Peak III, due to the asymmetric stretch of $W=O_d$ moieties, exhibits a shift of about 30 cm^{-1} V^{-1}, roughly in accord with previous work on the well-studied chemisorbed system CO on Pt (and other metals) with CO at high surface coverage.[72−75] On the other hand, peak IV exhibits a somewhat larger Stark shift. As discussed above, the molecule may be interacting with the surface primarily through $W-O_b-W$ and $W-O_c-W$ bridging modes. Since peak IV has some $W-O_b-W$ asymmetric stretch character as shown in Table 1, the larger Stark shift observed for this peak could be a manifestation of these $W-O_b-W$ modes being closer to the surface than modes associated with $W=O_d$.

In the SERS, Figure 8 shows that the magnitude of the Stark shift for peaks III and VI differs as well, with the Stark shift for peak VI much larger. Since peak VI is primarily due to modes associated with $W-O_c-W$, we again speculate that the molecule is interacting with the surface predominantly through W−O−W bridges. The exceptionally large magnitude of the shift observed for peak VI, between about 90 and 150 cm^{-1} V^{-1}, could be due to $W-O_c-W$ modes moving closer to the surface via rotation as suggested above in Figure 12b. We note that Stark shifts of this magnitude have been observed previously, where values of up to 120 cm^{-1} V^{-1} were found for NO on Rh(111) under certain circumstances.[73]

Interestingly, linear Stark shifts are not observed at all potentials in either the IRRAS or the SERS. The linear regions are roughly over the range where voltammetric waves are expected (−0.2 V) or present (−0.44 V) on Ag, as seen in Figure 2. Since vibrational Stark shifts generally reflect changes in chemical bonding between an adsorbate and the surface as well as classical electrostatic effects due to the changing electric field,[73,74,76] the linear regions of the plots in Figures 5 and 8 may correspond to potential-dependent changes in the surface bonding. The strong sensitivity of the vibrational frequency on the surface potential may be indicative of strong adsorbate−surface bonding (chemisorption) in our system.[73]

4.3.3.Correlation with Voltammetry—The Missing Wave. The above analysis suggests that the molecule is reorienting on the surface in the potential region where the first voltammetric wave is expected. This reorientation has specific spectroscopic consequences, but it also has consequences in the voltammetry. If the molecule is reduced immediately on contact with the Ag surface, then it is not surprising that the first reduction is not observed in the CV on the Ag surface. The question then shifts to the nonappearance of the concomitant oxidation wave on the anodic sweep. As the potential is moved more positive, the anion reorients back from its tilted configuration shown in Figures 11b and 12b to achieve greater coordination with the more positive surface, as was the case initially as shown in Figures 11a and 12a. This increased coordination uses electron density that would otherwise flow to oxidize the molecule. Correspondingly, no anodic wave is seen in the CV; rather, electron density flows out of the molecule but into Ag−O bonds rather than into the surface itself.

4.3.4. Peak IV Behavior at Anodic Potentials. As noted above, the behavior of peak IV is anomalous when compared with the other bands observed in the SERS on Ag. This peak is only present at relatively positive potentials and grows in dramatically positive of +0.2 V to dominate the spectrum at +0.3 V in Figure 7. In a previous study,[36] we showed that upon excursion to negative potentials, an irreversible anodic wave appeared around +0.02 V on the subsequent anodic sweep in the CV. It was speculated that this wave was due to oxidation of decomposition products of the reduced, adsorbed $Ag-SiW_{12}O_{40}$ complex. Although the exact nature of peak IV is unknown, this band might be correlated with the anodic wave seen at positive potentials in the CV. In particular, peak IV may be due to the initial stages of reoxidation of the complex. This would be a substantial positive shift in the oxidation wave relative to its position on HOPG or Au, as discussed previously.[36]

4.4. Comparison with Au. SERS of α-$[SiW_{12}O_{40}]^{4-}$ on a Au surface evince many of the same features as seen on the Ag surface regarding spectral shape and position of peaks. This suggests that the mode of association of α-$[SiW_{12}O_{40}]^{4-}$ with Ag and Au surfaces is similar. Indeed, STM images of α-$[SiW_{12}O_{40}]^{4-}$ associated with Au surfaces are similar to those obtained on Ag.[29] However, the peaks observed on Au show no potential dependence and only weak changes in relative intensity. This evidence, in contrast to that observed on Ag, suggests that the interaction of α-$[SiW_{12}O_{40}]^{4-}$ with the Au surface is relatively weak compared to the situation on Ag. This is in agreement with earlier STM[29] and electrochemical studies.[25,36]

Other details in the SERS on Au support the assertion that α-$[SiW_{12}O_{40}]^{4-}$ is more weakly bound on Au. First, the intensity of peak II, relative to other peaks in the spectra, is generally greater on Au compared with Ag. Since this peak is due to $W=O_d$ symmetric stretch modes, greater intensity on Au may be a consequence of weaker adsorption on this surface when compared to Ag. Second, note that peak VI is essentially absent at all potentials on the Au surface. This peak, while not present in the Raman of the solid material, is prominent on Ag as discussed above. The presence of this peak with the Ag surface-confined species may be a consequence of the strong interaction between the surface and the adsorbed polyoxometalate. Although the potential range is more limited in the Au study, this peak might still be expected to be present, as it is on Ag, even at 0 V and more positive potentials, if there is a strong interaction between the adsorbate and the surface. The absence of peak VI on Au lends further credence to the weak interaction on this surface.

If the polyoxometalate is reduced on the Ag surface, then some Ag has likely been oxidized, as suggested by other work.[67] If the strong adsorption observed on the Ag surface were to be present on the Au surface as well, one might expect some oxidation of Au on the surface. However, oxidation of Au occurs at potentials much more positive than oxidation of Ag, which

likely accounts for the different behavior observed for these two surfaces. We therefore anticipate a strong interaction between α-$[SiW_{12}O_{40}]^{4-}$ and Cu surfaces due to the less stringent potentials required for Cu oxidation.

5. Conclusions

Surface-sensitive vibrational spectroscopy shows that α-$[SiW_{12}O_{40}]^{4-}$ adsorbs intact on Ag and Au surfaces. Assignment of vibrational modes and examination of peak behavior as a function of potential imply that α-$[SiW_{12}O_{40}]^{4-}$ interacts with the surface through W−O−W bridging modes. Peak behavior, in terms of both intensity changes and Stark shifts, was often distinct for different peaks within one type of spectroscopy. Furthermore, the same peak sometimes behaved differently in the PM-IRRAS when compared with the SERS. Analysis of individual peaks and their corresponding modes allowed us to propose a model for the behavior of the molecule as a function of potential. This model, a rotation on the surface at negative potentials, also accounts for the missing voltammetric wave on Ag. It is likely that the polyoxometalate species is reduced on the surface, even at potentials positive of the first redox wave of α-$[SiW_{12}O_{40}]^{4-}$. Although adsorption geometries are similar on Ag and Au, vibrational spectroscopy of α-$[SiW_{12}O_{40}]^{4-}$ on these two surfaces shows several differences, with the implication being that the interaction of α-$[SiW_{12}O_{40}]^{4-}$ with Au surfaces is much weaker than its interaction with Ag surfaces.

Acknowledgment. Much of the α-$H_4SiW_{12}O_{40}\cdot nH_2O$ used in this work was synthesized by Jason Powell. We thank Nolan Flynn for assistance with acquisition of initial Raman data. We thank Rick Haasch for assistance with XPS, which was carried out in the Center for Microanalysis of Materials, University of Illinois, which is partially supported by the U.S. Department of Energy under Grant DEFG02-91-ER45439. The Laser Laboratory is funded by the Department of Energy through the Materials Research Laboratory at the University of Illinois. XL and J.K. thank the Department of Chemistry for financial support in the form of a Carl Shipp Marvel Fellowship and University Block Grant, respectively. This work was funded by the National Science Foundation (CHE-02-37683), which is gratefully acknowledged.

References and Notes

(1) Pope, M. T. *Heteropoly and Isopoly Oxometalates*; Springer-Verlag: Berlin, 1983.
(2) *Polyoxometalates: From Platonic Solids to Anti-Retroviral Activity*; Pope, M. T.; Müller, A., Eds.; Kluwer: Boston, 1994.
(3) *Polyoxometalate Chemistry From Topology via Self-Assembly to Applications*; Pope, M. T.; Müller, A., Eds.; Kluwer: Boston, 2001.
(4) *Polyoxometalate Chemistry for Nano-Composite Design*; Yamase, T.; Pope, M. T., Eds.; Kluwer/Plenum: New York, 2002.
(5) Sadakane, M.; Steckhan, E. *Chem. Rev.* **1998**, *98*, 219−237.
(6) Baker, L. C. W.; Glick, D. C. *Chem. Rev.* **1998**, *98*, 3−49.
(7) Teze, A.; Herve, G. *Inorg. Synth.* **1990**, *27*, 85−96.
(8) Gouzerh, P.; Proust, A. *Chem. Rev.* **1998**, *98*, 77−111.
(9) Weinstock, I. A. *Chem. Rev.* **1998**, *98*, 113−170.
(10) Kozhevnikov, I. V. *Chem. Rev.* **1998**, *98*, 171−198.
(11) Mizuno, N.; Misono, M. *Chem. Rev.* **1998**, *98*, 199−217.
(12) Katsoulis, D. E. *Chem. Rev.* **1998**, *98*, 359−387.
(13) Weinstock, I. A.; Barbuzzl, E. M. G.; Wemple, M. W.; Cowan, J. J.; Reiner, R. S.; Sonnen, D. M.; Heintz, R. A.; Bond, J. S.; Hill, C. L. *Nature (London)* **2001**, *414*, 191−195.
(14) Kamata, K.; Yonehara, K.; Sumida, Y.; Yamaguchi, K.; Hikichi, S.; Mizuno, N. *Science* **2003**, *300*, 964−966.
(15) Rocchiccioli-Deltcheff, C.; Fournier, M.; Franck, R.; Thouvenot, R. *Inorg. Chem.* **1983**, *22*, 207−216.
(16) Klemperer, W. G.; Wall, C. G. *Chem. Rev.* **1998**, *98*, 297−306.
(17) Keita, B.; Nadjo, L. *J. Electroanal. Chem.* **1985**, *191*, 441−448.
(18) Wang, B.; Dong, S. *J. Electroanal. Chem.* **1992**, *328*, 245−257.
(19) Keita, B.; Nadjo, L. *J. Electroanal. Chem.* **1993**, *354*, 295−304.
(20) Rong, C.; Anson, F. C. *Inorg. Chim. Acta* **1996**, *242*, 11−16.
(21) Song, I. K.; Kaba, M. S.; Coulston, G.; Kourtakis, K.; Barteau, M. A. *Chem. Mater.* **1996**, *8*, 2352−2358.
(22) Song, I. K.; Kaba, M. S.; Barteau, M. A. *J. Phys. Chem.* **1996**, *100*, 17528−17534.
(23) Kaba, M. S.; Song, I. K.; Barteau, M. A. *J. Phys. Chem.* **1996**, *100*, 19577−19581.
(24) Kaba, M. S.; Song, I. K.; Barteau, M. A. *J. Vac. Sci. Technol., A* **1997**, *15*, 1299−1304.
(25) Keita, B.; Nadjo, L.; Belanger, D.; Wilde, C. P.; Hilaire, M. *J. Electroanal. Chem.* **1995**, *384*, 155−169.
(26) Rong, C.; Anson, F. C. *Anal. Chem.* **1994**, *66*, 3124−3130.
(27) Ge, M.; Zhong, B.; Klemperer, W. G.; Gewirth, A. A. *J. Am. Chem. Soc.* **1996**, *118*, 5812−5813.
(28) Ge, M.; Gewirth, A. A.; Klemperer, W. G.; Wall, C. G. *Pure Appl. Chem.* **1997**, *69*, 2175−2178.
(29) Ge, M.; Niece, B. K.; Wall, C. G.; Klemperer, W. G.; Gewirth, A. A. *Mater. Res. Soc. Symp. Proc.* **1997**, *451*, 99−108.
(30) Lee, L.; Wang, J. X.; Adzic, R. R.; Robinson, I. K.; Gewirth, A. A. *J. Am. Chem. Soc.* **2001**, *123*, 8838−8843.
(31) Ingersoll, D.; Kulesza, P. J.; Faulkner, L. R. *J. Electrochem. Soc.* **1994**, *141*, 140−147.
(32) Kuhn, A.; Anson, F. C. *Langmuir* **1996**, *12*, 5481−5488.
(33) Cheng, L.; Niu, L.; Gong, J.; Dong, S. *Chem. Mater.* **1999**, *11*, 1465−1475.
(34) Kuhn, A.; Mano, N.; Vidal, C. *J. Electroanal. Chem.* **1999**, *462*, 187−194.
(35) Liu, S.; Tang, Z.; Shi, Z.; Niu, L.; Wang, E.; Dong, S. *Langmuir* **1999**, *15*, 7268−7275.
(36) Lee, L.; Gewirth, A. A. *J. Electroanal. Chem.* **2002**, *522*, 11−20.
(37) Kim, J.; Gewirth, A. A. *Langmuir* **2003** *19*, 8934−8942.
(38) Powell, J. D. Ph.D. Thesis, University of Illinois at Urbana−Champaign, Urbana, IL, 2001.
(39) Powell, J. D.; Gewirth, A. A.; Klemperer, W. G. In *Polyoxometalate Chemistry From Topology via Self-Assembly to Applications*; Pope, M. T., Müller, A., Eds.; Kluwer: Boston, 2001; pp 329−334.
(40) Weaver, M. J.; Zou, S. Z.; Chan, H. Y. H. *Anal. Chem.* **2000**, *72*, 38A−47A.
(41) Weaver, M. J. *J. Raman Spectrosc.* **2002**, *33*, 309−317.
(42) Campion, A.; Kambhampati, P. *Chem. Soc. Rev.* **1998**, *27*, 241−250.
(43) Hamelin, A.; Doubova, L.; Stoicoviciu, L.; Trasatti, S. *J. Electroanal. Chem. Interfacial Electrochem.* **1988**, *244*, 133−145.
(44) Will, T.; Dietterle, M.; Kolb, D. M. In *Nanoscale Probes of the Solid/Liquid Interface*; Gewirth, A. A., Siegenthaler, H., Eds.; Kluwer: Boston, 1995; pp 137−162.
(45) Li, X.; Gewirth, A. A. *J. Am. Chem. Soc.* **2003**, *125*, 7086−7099.
(46) Leung, L. W. H.; Gosztola, D.; Weaver, M. J. *Langmuir* **1987**, *3*, 45−52.
(47) Feilchenfeld, H.; Gao, X. P.; Weaver, M. J. *Chem. Phys. Lett.* **1989**, *161*, 321−326.
(48) Gao, P.; Gosztola, D.; Leung, L. W. H.; Weaver, M. J. *J. Electroanal. Chem. Interfacial Electrochem.* **1987**, *233*, 211−222.
(49) Stolberg, L.; Lipkowski, J.; Irish, D. E. *J. Electroanal. Chem. Interfacial Electrochem.* **1991**, *300*, 563−584.
(50) Oh, I.; Biggin, M. E.; Gewirth, A. A. *Langmuir* **2000**, *16*, 1397−1406.
(51) Biggin, M. E.; Gewirth, A. A. *J. Electrochem. Soc.* **2001**, *148*, C339−C347.
(52) Cerius^2 software release 4.8, Molecular Simulations, Inc.: San Diego, 2002.
(53) Herve, G. *Ann. Chim. (Paris)* **1971**, *6*, 219−227.
(54) Herve, G. *Ann. Chim. (Paris)* **1971**, *6*, 287−296.
(55) Pope, M. T.; Varga, G. M., Jr. *Inorg. Chem.* **1966**, *5*, 1249−1254.
(56) Porter, M. D.; Karweik, D. H.; Kuwana, T.; Theis, W. B.; Norris, G. B.; Tiernan, T. O. *Appl. Spectrosc.* **1984**, *38*, 11−16.
(57) Nakamoto, K. *Infrared and Raman Spectra of Inorganic and Coordination Compounds*, 3rd ed.; Wiley: New York, 1978.
(58) Buckley, R. I.; Clark, R. J. H. *Coord. Chem. Rev.* **1985**, *65*, 167−218.
(59) Bridgeman, A. J. *Chem. Phys.* **2003**, *287*, 55−69.
(60) Siiman, O.; Feilchenfeld, H. *J. Phys. Chem.* **1988**, *92*, 453−464.
(61) Cao, P.; Gu, R.; Tian, Z. *J. Phys. Chem. B* **2003**, *107*, 769−777.
(62) Morzyk-Ociepa, B.; Michalska, D. *Spectrochim. Acta, Part A* **2003**, *59A*, 1247−1254.
(63) Niaura, G.; Jakubenas, R. *J. Electroanal. Chem.* **2001**, *510*, 50−58.
(64) Ratajczak, H.; Barnes, A. J.; Bielanski, A.; Lutz, H. D.; Müller, A.; Pope, M. T. In *Polyoxometalate Chemistry From Topology via Self-Assembly to Applications*; Pope, M. T., Müller, A., Eds.; Kluwer: Boston, 2001; pp 101−116.
(65) Thouvenot, R.; Fournier, M.; Franck, R.; Rocchiccioli-Deltcheff, C. *Inorg. Chem.* **1984**, *23*, 598−605.

(66) Day, V. W.; Klemperer, W. G. *Science* **1985**, *228*, 533−541.
(67) Lee, L. Ph.D. Thesis, University of Illinois at Urbana−Champaign, Urbana, IL, 2001.
(68) Ni, C.-L.; Anson, F. C. *Inorg. Chem.* **1985**, *24*, 4754−4756.
(69) NIST X-ray Photoelectron Spectroscopy Database 3.3 ed., http://srdata.nist.gov/xps/, 2003.
(70) Fournier, M.; Rocchiccioli-Deltcheff, C.; Kazansky, L. P. *Chem. Phys. Lett*. **1994**, *223*, 297−300.
(71) Artero, V.; Proust, A. *Eur. J. Inorg. Chem.* **2000**, 2393−2400.
(72) Lambert, D. K. *Electrochim. Acta* **1996**, *41*, 623−630.
(73) Weaver, M. J.; Zou, S.; Tang, C. *J. Chem. Phys.* **1999**, *111*, 368−381.
(74) Koper, M. T. M.; van Santen, R. A.; Wasileski, S. A.; Weaver, M. J. *J. Chem. Phys.* **2000**, *113*, 4392−4407.
(75) Weaver, M. J.; Wasileski, S. A. *Langmuir* **2001**, *17*, 3039−3043.
(76) Zou, S.; Weaver, M. J. *J. Phys. Chem.* **1996**, *100*, 4237−4242.